Check for
updates

The Energy of a Tsunami Generated by Dynamic Uplift of the Ocean Bottom. I. Analytical Solutions

EMILE A. OKAL[1]

Abstract—Based on a simple physical model, we derive a formula for the energy radiated into a tsunami by a dynamic deformation of the ocean floor. We use the analytical solutions developed by J.L. Hammack, Jr. (1972, Tsunamis – A model of their generation and propagation, *Ph.D. Dissertation*, 261 pp., California Institute of Technology, Pasadena) to show that, in addition to its expected dependence on the source rise time, and even in the limiting case of an instantaneous source, the energy of the tsunami is controlled by the ratio of water depth to source size. For very large earthquakes, these results have no impact on the time-honored approximation which uses the static deformation of the ocean floor as a set of initial conditions of the surface displacements for numerical simulations, but they provide insight into the theoretical limits of this practice.

Keywords: Tsunami energy, theoretical hydrodynamics, Shallow water approximation.

1. Introduction

1.1. Background and Motivation

In most numerical simulations of tsunamis generated by earthquakes, the seismic source is taken as an instantaneous deformation of the ocean floor, directly transposed to the ocean surface and then used as an initial condition for the hydrodynamic equations governing the propagation of the tsunami (*e.g.*, Titov et al. 2016). In reality, this time-honored practice constitutes a "static" approximation, as documented, for example, by the recent work of Derakhti et al. (2019) who have examined in detail the influence of dynamic parameters such as rise time of the parent earthquake on tsunami amplitudes.

[1] Department of Earth and Planetary Sciences, Northwestern University, Evanston, IL 60208, USA. E-mail: emile@earth.northwestern.edu

However, this approach remains legitimate in the overwhelming majority of cases since the duration of an earthquake source is generally negligible compared with the time it takes a tsunami to propagate over the dimension of its source area.

It is attractive, from the standpoint of global Physics, to characterize a tsunami through its energy E^{TSU} initially delivered at the source, since it provides an integrated estimate of the size of the phenomenon, and allows a meaningful comparison with other physical processes. Our goal in the present paper will be to investigate the influence of dynamic parameters on E^{TSU} in the simplified model of the uplift of a plug of ocean floor. We conclude that, in addition to rise time, the ratio of water depth to source size can play a crucial role in controlling the energy available to the development of the tsunami, but we confirm that for large earthquakes, the static approximation remains valid.

1.2. Previous Work on Tsunami Energy

Attempts to quantify the energy transported by a tsunami through an oceanic basin can be traced back to Iida (1963) and Munk (1963). In a landmark contribution. Kajiura (1981, Eq. (12)) obtained a formula expressing the energy of a tsunami generated by an instantaneous double-couple dislocation buried in a elastic half-space underlying an oceanic column, which Okal (2003) has rewritten as

$$E^{Kaj.} = \frac{1}{2^{4/3}} \frac{\rho g}{\mu^{4/3}} \varepsilon_{max}^{2/3} \cdot M_0^{4/3} \cdot F_{Kaj.} \qquad (1)$$

where ρ is the density of water, μ the rigidity of the Earth, g the acceleration of gravity, M_0 the seismic moment of the source, and ε_{max} the elastic strain release; $F_{Kaj.}$ is a non-dimensional average of the

square of the vertical displacement of the ocean floor above the source, scaled to the seismic slip on the fault. The two main properties of (1) are the growth of the energy as $M_0^{4/3}$, *i.e.,* faster than the seismic moment, and its independence on the depth h of the oceanic water column. Okal (2003, Eq. (57)) showed further that (1) is in general agreement with an estimate of the energy based on the representation of the tsunami as a branch of the normal modes of the Earth, following Ward (1980):

$$E^{Modes} \;=\; \frac{0.22\,\rho\,g}{\mu^{4/3}}\;\varepsilon_{max}^{2/3}\,M_0^{4/3} \;=\; 0.22\,\rho\,g\,\varepsilon_{max}^{2/3}\cdot P_0^{4/3}$$

(2)

where $P_0 = S\,\Delta u$ is the so-called "potency" of the source, with units of volume (King 1978; Ben-Menahem and Singh 1981).

Later studies of tsunami energy consisted mainly of interpreting tidal gauge records in terms of the total energy radiated into the [Pacific] Ocean, and of studying its decay with time through scattering and absorption at coastal boundaries, as initially proposed by Munk (1963). Van Dorn (1984) and later Rabinovich et al. (2013) expressed tsunami energies through a "tsunami energy index" E_0 (with dimensions of surface) scaling the square of the tsunami energy, integrated from its amplitude, to the size of the oceanic basin, and to the volumetric weight ρg of the ocean. When combined with (2), this leads to

$$E_0 \;\approx\; \frac{1}{20}\,\varepsilon_{max}^{2/3}\,\frac{P_0^{4/3}}{a^2}$$

(3)

where a is the radius of the Earth, and taking the surface of the Pacific Ocean as 1/3 that of the whole Earth. Equation (3) predicts values of $E_0 = 1100$ and 430 cm^2 for the 1960 Chile and 1964 Alaska tsunamis, respectively, in good agreement with those obtained by Van Dorn (1984), and of 125, 43, and 2 cm^2, for the 2009 Samoa, 2010 Chile and 2011 Tohoku events, generally compatible with the upper bounds proposed by Rabinovich et al. (2013).

Dutykh and Dias (2009) later studied the evolution of the tsunami energy with time, by considering differential equations governing the vertical integral over the ocean column of the volumetric densities of kinetic and gravitational energy.

Our approach here will be to consider the energetics of the dynamic uplift of a plug at the ocean floor, under scenarios for which analytical solutions to the equations of hydrodynamics are available.

2. The Formula

We consider here the two-dimensional model of a flat oceanic layer of thickness h (Fig. 1). The system is initially at equilibrium, and at time $t = 0_+$, a plug of elementary surface dS is pushed upwards, the deformation ceasing at time T; similar results would be obtained for a downwards motion ($\zeta < 0$). At any given time t ($0 < t \le T$), the plug has moved by $\zeta(t)$ and the ocean surface above it has been deformed by $\eta(t)$, which is the amplitude of the tsunami generated above the plug by the deformation. Note that we *do not assume* that $\eta = \zeta$.

In order to move upwards, the plug has to work against the local pressure P which is the sum of the original pressure at equilibrium, $P_{eq} = \rho\,g\,h$, and of an overpressure $p^*(t)$, itself the combination of the effect of moving the floor up by $\zeta(t)$ and of the dynamic overpressure $p(t)$ which accompanies the tsunami:

$$P(t) \;=\; P_{eq} + p^*(t) \;=\; P_{eq} - \rho\,g\,\zeta(t) + p(t)$$

(4)

The plug is then exerting on the water layer a force directed upwards $dF = P\,dS$ whose elementary work during deformation from ζ to $\zeta + d\zeta$ is

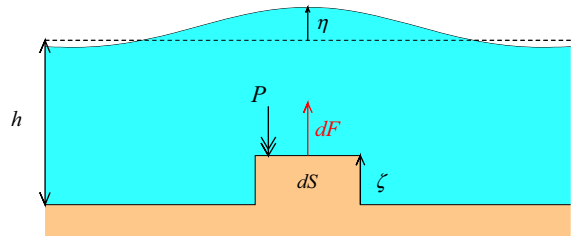

Figure 1

Schematics of the dynamic uplift of a plug of section dS in an ocean of depth h. At the time considered, the amplitude of the deformation is ζ, and the displacement of the surface above it is η. The force dF works against the pressure $[P = \rho\,g\,(h - \zeta) + p]$. Note that $\eta \neq \zeta$

$$dW = dF \cdot d\zeta = [\rho g (h - \zeta) + p] \cdot dS \cdot d\zeta \tag{5}$$

The total energy transmitted to the water column during the deformation is the integral of (5):

$$dE^{total} = \int_0^{\zeta(T)} \rho g [h - \zeta(t)] \cdot dS \cdot d\zeta + \int_0^T p(t) \cdot dS \cdot \frac{d\zeta}{dt} \cdot dt \tag{6}$$

Regardless of the time history of the function $\zeta(t)$, the first integral amounts to

$$dE^{Pot.} = \rho \, dS \, \zeta(T) \, [h - \zeta(T)/2] \, g \tag{7}$$

which represents the potential energy gained by the mass of displaced water, $\rho \, dS \, \zeta(T)$, between its initial position in which its center of mass was at altitude $\zeta(T)/2$ above the ocean floor, and its final resting position where it is distributed along an infinitely thin film of water at the surface of the ocean (assumed infinite along x), at altitude h above the undeformed ocean floor.

The second integral in (6), which is the work performed in excess of this eventual change in potential energy, is transferred to an oscillation of the water column and represents the energy of the tsunami:

$$dE^{TSU} = dE^{total} - dE^{Pot.} = dS \int_0^T p \frac{d\zeta}{dt} \cdot dt \tag{8}$$

which can be generalized to the three-dimensional case of an extended area Σ of deformation of the ocean floor where ζ can vary laterally:

$$E^{TSU} = \int \int_\Sigma dx \, dy \int_0^T p(x, y; t) \frac{\partial \zeta(x, y; t)}{\partial t} \cdot dt \tag{9}$$

The traditional approach (Kajiura 1981) makes two approximations. First it assumes that $\eta(x, y; t)$ is identically equal to $\zeta(x, y; t)$, i.e., that during the deformation, the water displaced at the bottom is simply transferred to the surface where it creates a hump of identical shape; in other words, the thickness of the water column is always h, for all (x, y) and $t \leq T$. Second, it assumes that the dynamic overpressure $p(x, y; t)$ is simply the hydrostatic term

$$p(x, y; t) = \rho g \eta(x, y; t) \tag{10}$$

This leads to the classic formula (Okal and Synolakis 2003; Dutykh and Dias 2009)

$$E^{Static} = \frac{1}{2} \rho g \int \int_\Sigma [\zeta(x, y; T)]^2 \cdot dx \, dy \tag{11}$$

where $\zeta(x, y; T)$ is the final "static" deformation of the ocean floor. Note the proportionality of the energy to Σ and ζ^2, which under scaling laws (Geller 1976), grows globally as $M_0^{4/3}$, in agreement with the results of Kajiura (1981) and Okal (2003); we also verify that (11) is obviously unchanged for a downward motion ($\zeta < 0$).

A clear illustration of the limitation of the first approximation is given e.g., by Derakhti et al. (2019), who confirmed that slow deformations will generally lead to surface amplitudes η smaller than the bottom deformation ζ. Under such conditions, but assuming that the second approximation (10) still holds, Equation (9) becomes

$$E^{TSU} = \rho g \int \int_\Sigma dx \, dy \int_0^T \eta(x, y; t) \frac{\partial \zeta(x, y; t)}{\partial t} \cdot dt = E^{SWA} \tag{12}$$

The limitation of the second approximation is rooted in the fact that, for sufficiently high frequencies (or wavenumbers k), the tsunami eigenfunction attenuates with depth. This is illustrated for example by the fact that submarines below about 150 m do not feel weather-induced surface swell. Under this model, and in the case of a monochromatic wave with wavenumber k, the overpressure p now taken at the depth $(h - \zeta)$ becomes (e.g., Gill 1982; Dean and Dalrymple 2000):

$$p(x, y; t) = \rho g \frac{\eta(x, y; t)}{\cosh k(h - \zeta)} \approx \rho g \frac{\eta(x, y; t)}{\cosh kh} \tag{13}$$

The term $(1/\cosh kh)$ has been called a "pressure response factor" by Dean and Dalrymple (2000). It is clear that it quantifies the dispersion of the wave and goes to 1 when $kh \to 0$, i.e., under the Shallow-Water Approximation [hereafter SWA]. For this reason, we refer to E^{TSU} given by Eq. (12) as E^{SWA}.

Saito (2017) has also discussed limitations on the relation between p and η outside the SWA.

A number of fundamental physical properties are inherent in the above derivation. First, the origin of the tsunami rests in the thermodynamically irreversible character of the deformation: at any given time t and because of the term p in (4) and hence (9), the total work spent is larger than strictly necessary if the system was constantly in equilibrium with a thickness $(h - \zeta(t))$. This is similar to the case of extending a spring by hanging a constant mass at its extremity, which results in an extra work of its weight, over and beyond the (elastic) potential energy eventually stored in the extended spring at equilibrium, thus forcing the oscillation of the spring. In both instances, it is easily verified that the energy thus "wasted" (in the oscillation of tsunami waves or of the spring) is reduced by a factor of 2 if the deformation is decomposed into two halves, separated by enough time to allow the oscillation to decay and the system to reach an intermediate equilibrium. It would eventually vanish in the limit of a infinite number of elementary processes, in which case the deformation would then become *reversible*.

Second, this last remark underlines the thermodynamic relationship between a fast transformation and its irreversible character, expressed as the amount of energy wasted in the process. As investigated in detail, *e.g.,* by Derakhti et al. (2019), the amplitude of a tsunami over a rising plug decreases strongly with increasing rise time of the deformation. In lay terms, a tsunami is generated because the ocean floor deforms too fast, and as such irreversibly. In particular, no tsunami is generated during the interseismic interval of the tectonic cycle, when the ocean bottom, locked at the interplate contact, buckles at tectonic rates of a few cm/yr, even though the total deformation accumulated between two mega-thrust earthquakes is of course of the same amplitude (but with opposite sign) as that occurring during such events; but one scenario takes over a hundred years, the other a few tens of seconds.

3. Application to Analytical Models

The question of the exact history of the height of the ocean surface, η, during a deformation of the ocean floor ζ of finite duration has been investigated

both theoretically and numerically. In the present paper, we will consider two scenarios for which Hammack (1972) derived relatively simple analytical solutions to the equations of hydrodynamics. Application of our results in the context of numerical solutions will be the subject of a later publication.

3.1. The Two-dimensional Case

Hammack (1972) first considers a two-dimensional ocean of depth h, with a linear plug of length $2b$ centered at $x = 0$ (Fig. 2; red labels). The model has translational symmetry in the y direction, which is dropped from all further calculations, and mirror symmetry about $x = 0$. His strategy consists of applying a spatial Fourier transform ($x \rightarrow k$) followed by a temporal Laplace transform ($t \rightarrow s$). The surface displacement is then obtained as (Hammack 1972; Eq. (3.29)):

$$\eta(x, t) = \frac{1}{2\pi} \int_{-\infty}^{\infty} \frac{e^{-ikx}}{\cosh kh} \left[\frac{1}{2i\pi} \int_{Br.} e^{st} \cdot \frac{s^2}{s^2 + \omega^2} \widetilde{\overline{\zeta}}(k; s) \cdot ds \right] \cdot dk \tag{14}$$

where for each value of k, the angular frequency ω is given by the classic dispersion relation
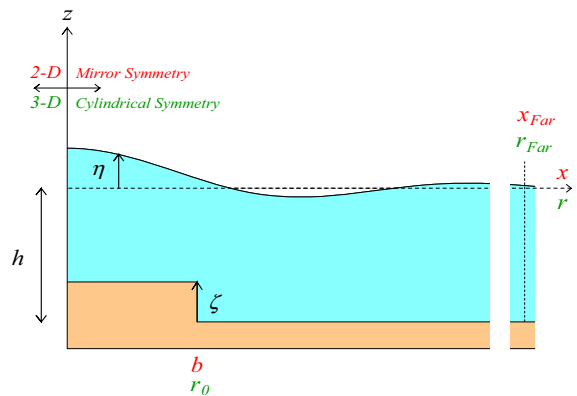

Figure 2
Sketches of the models used by Hammack (1972). The two-dimensional model, labeled in red, has translational symmetry in the y direction perpendicular to the figure, and mirror symmetry about $x = 0$. The cylindrical model, labeled in green, has azimuthal symmetry about the axis z. In both instances, a plug of ocean floor (light brown) is uplifted into the ocean column (blue), of initial thickness h. At any given time, the uplift of the plug is ζ, and the deformation of the surface η. The far-field energy flux is computed at the [large] range x_{Far} (or r_{Far})

$$\omega^2 \ = \ g\,k \ \cdot \ \tanh\,(kh) \ , \qquad (15)$$

$\widetilde{\widetilde{\zeta}}\,(k;\,s)$ is the double Fourier-Laplace transform of the displacement $\zeta\,(x;\,t)$, and the integral over s is taken along a Bromwich contour (Boas 1983; p. 662). In general, the displacement ζ is taken as independent of x inside the plug.

We will consider here the cosine time function used by Hammack (1972), with a finite duration T, which provides a realistic representation of a seismic source. The space-time history of deformation of the bottom of the ocean is then given by

$$\zeta\,(x;\,t) \ = \ \zeta_0\,H\,(b^2 \ - \ x^2)$$
$$\cdot \ \left[\frac{1}{2}\,(1 \ - \ \cos\,\kappa t)\,H\,[t\,(T \ - \ t)] \ + \ H\,(t \ - \ T)\right] \qquad (16)$$

where H is the Heaviside function, and $\kappa \ = \ \pi/T$ characterizes the rise time of the source, as shown on Fig. 3. Note that this time function is also used by Derakhti et al. (2019) with the notation t_r for the rise time T. The derivative $\dot{\zeta}$ takes the form

$$\dot{\zeta}\,(x;\,t) \ = \ \frac{1}{2}\,\zeta_0\,\kappa \ \cdot \ H\,(b^2 \ - \ x^2) \ \cdot \ H\,[t\,(T \ - \ t)] \ \cdot \ \sin\,\kappa t \qquad (17)$$

and Eq. (14) then becomes a simple integral over k (Hammack 1972; Eq. (3.41)):

$$\eta\,(x;\,t) \ = \ \frac{\zeta_0}{\pi}\,\int_0^\infty \frac{\cos\,kx \ \sin\,kb}{k\,\cosh\,kh} \ \cdot \ \frac{\kappa^2}{\kappa^2 \ - \ \omega^2} \ \cdot$$
$$\cdot \ [\cos\,\omega t \ - \ \cos\,\kappa t \ + \ H\,(t \ - \ T)\,(\cos\,\omega\,(t \ - \ T)$$
$$+ \ \cos\,\kappa t)] \ \cdot \ dk \qquad (18)$$

where ω is given by (15). It can be verified that the integrand in (18) remains continuous when $\omega \ \to \ \kappa$.

$T = \pi/\kappa$

ζ_0

$\zeta\,(t)$

$\kappa = 0.045\ \text{s}^{-1}$
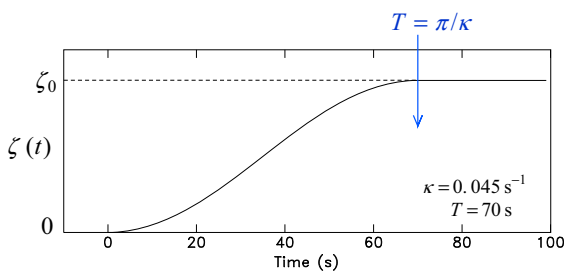$T = 70\ \text{s}$

0

0　　20　　40　　60　　80　　100
Time (s)

Figure 3
Example of a cosine source time function (16) used in this study

Since this integral is over wavenumber k, the dynamic pressure $p\,(x;\,t)$ can be obtained by simply factoring into the integrand the pressure response factor $(1/\cosh\,kh)$ defined in (13):

$$p\,(x;\,t) \ = \ \frac{\zeta_0\,\rho\,g}{\pi}\,\int_0^\infty \frac{\cos\,kx \ \sin\,kb}{k\,\cosh^2\,kh} \ \cdot \ \frac{\kappa^2}{\kappa^2 \ - \ \omega^2} \ \cdot$$
$$\cdot \ [\cos\,\omega t \ - \ \cos\,\kappa t \ + \ H\,(t \ - \ T)$$
$$(\cos\,\omega\,(t \ - \ T) \ + \ \cos\,\kappa t)] \ \cdot \ dk \qquad (19)$$

The value of E^{TSU} is then obtained by substituting (17) and (19) into (9):

$$E^{TSU} \ = \ \zeta_0\,\kappa \ \int_0^b dx \ \int_0^T p\,(x;\,t) \ \sin\,\kappa t \ \cdot \ dt \qquad (20)$$

In the present study, we investigate the dependence of E^{TSU} on the source rise time by considering 12 values of κ, geometrically spaced between 0.0093 and 5.24 s^{-1} (rise times π/κ from 338 to 0.6 s), for five values $h \ = \ 0.2, 0.5, 1, 2$ and 4 km of the ocean depth, and five values $b \ = \ 3, 5, 7, 10$ and 15 km of the half-width of the plug. We compute numerically the integrals (18) and (19) at 151 distances x, equally spaced between 0 (the center of the plug) and 15 km (the edge of the largest plug considered), and for 10,000 time steps, which are adjusted to the value of κ, in order to adequately sample the rise of the source. We then substitute (19) into (20), in which E^{TSU} now has dimensions of force (energy per unit length in the y direction). We scale the result to a similarly redimensioned version of (11):

$$E^{Static} \ = \ \frac{\rho\,g}{2}\,\int_{-b}^b dx\,[\zeta\,(x;\,T)]^2 \ = \ \rho\,g\,b\,\zeta_0^2 \quad (21)$$

and plot on Fig. 4 representative cases ($b \ = \ 3, 7$ and 15 km, respectively) of the ratio $(E^{TSU}\,/\,E^{Static})$ as solid lines color-coded for different ocean depths. In Fig. 5, the same values are plotted for selected depths h, color-coded for the various values of the half-source width b.

In addition, we also include (as similarly color-coded open squares) the values (E^{SWA}/E^{Static}) obtained under the SWA assumption that the over-pressure p simply takes its hydrostatic form (10).
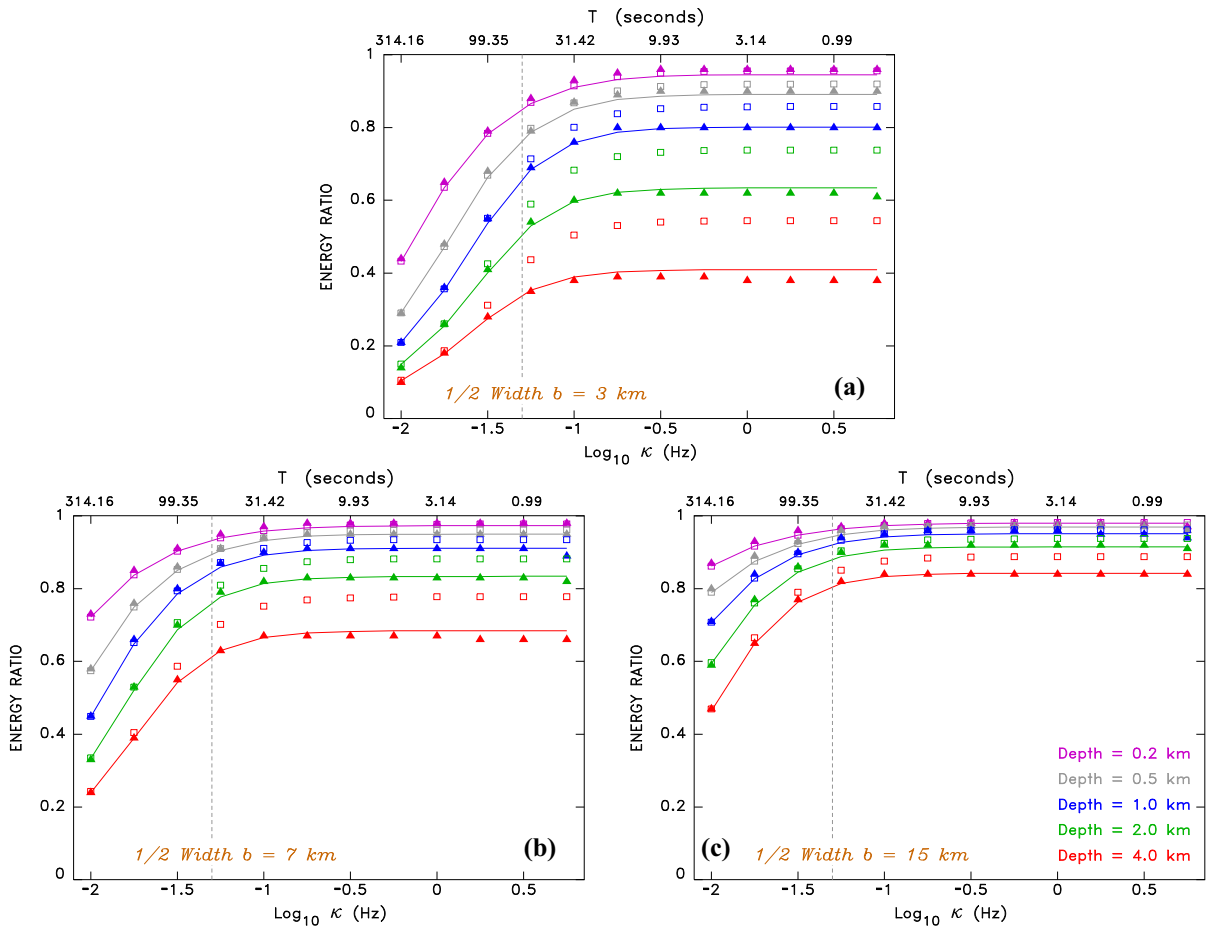
Figure 4
Plots of the ratio E^{TSU} / E^{Static} as a function of the parameter κ of the source, for representative values of the half-width b of a two-dimensional source: **a** 3 km; **b** 7 km and **c** 15 km. In each frame, lines of various colors relate to various depths of the oceanic column, from magenta (200 m) to red (4 km). The abscissa is linear in $\log_{10} \kappa$ with corresponding values of $T = \pi/\kappa$ shown along the top axis. Solid lines represent individual values computed using (19), (20) and (21); solid triangles represent far-field tsunami energies estimated independently (26). Open squares represent the Shallow-Water Approximation ratios E^{SWA} / E^{Static} computed using (12). The vertical gray dotted lines, corresponding to $T_t = 60$ s, identify the regime (to the left) where the rise time controls the dominant wavenumber K (see Sect. 4)

Next, we carry out an independent evaluation of the energy of the tsunami by considering a far-field value, x_{Far}, of the range x, and computing the integral over time of the energy flux through the wavefront at x_{Far}. This strategy is inspired by the classic algorithm for the computation of the energy radiated by a seismic source from teleseismic recordings of its P waves (Boatwright and Choy 1986).

Specifically, we prolong mathematically the solution (18) inside the water column ($z = 0$ at the surface, $-h$ at the bottom) to obtain the particle velocities v_x and v_z:

$$v_x(x, z; t) = \frac{\zeta_0}{\pi} \int_0^\infty \frac{\sin kx \sin kb}{k \cosh kh} \cdot \frac{\cosh k(h + z)}{\sinh kh} \cdot$$

$$\frac{\kappa^2}{\kappa^2 - \omega^2} \cdot$$

$$\cdot \left[\omega \sin \omega t - \kappa \sin \kappa t \right.$$

$$\left. + H(t - T)(\omega \sin \omega (t - T) + \kappa \sin \kappa t) \right] \cdot dk$$
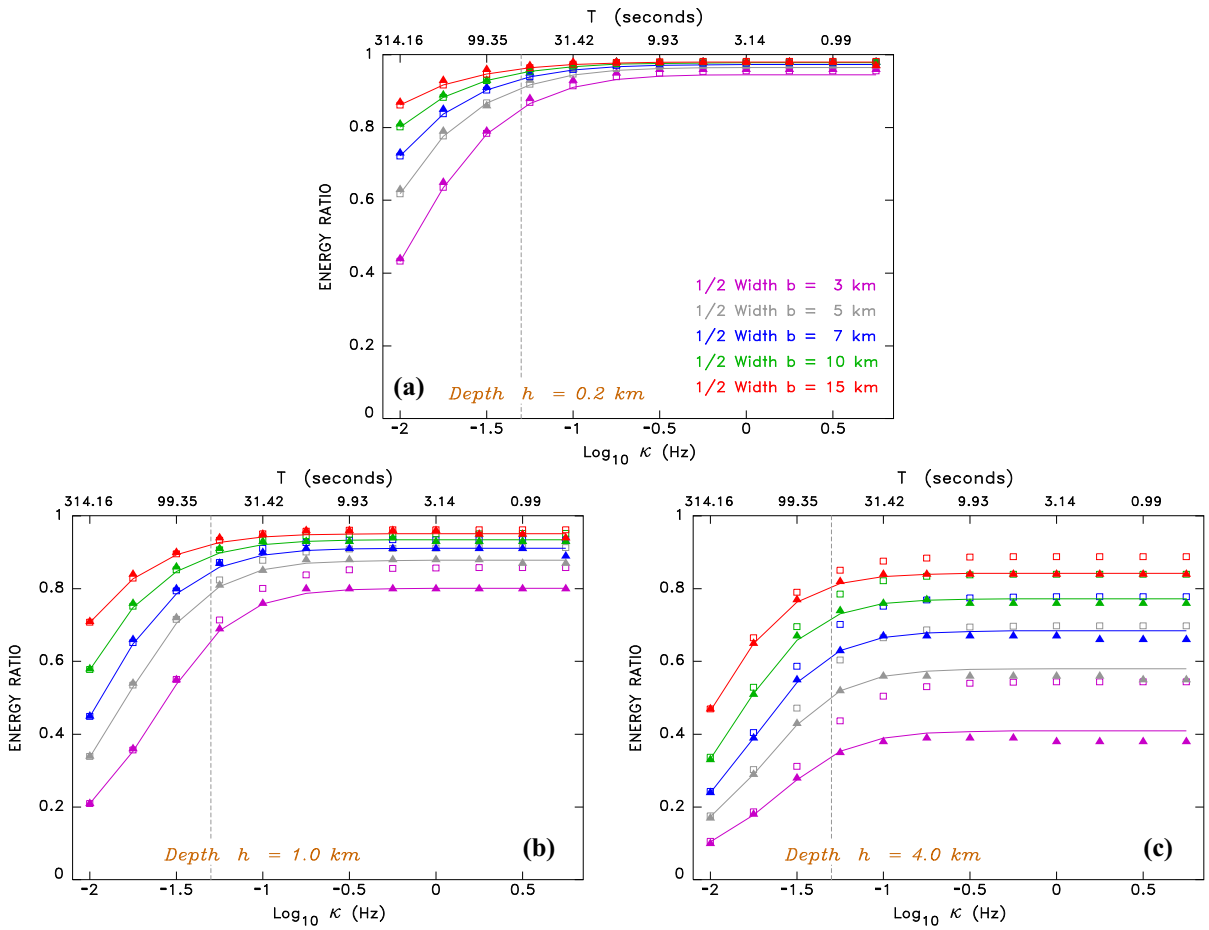
$$(22)$$

Figure 5
Same as Figure 4 for representative values of ocean depth, **a** 0.2 km, **b** 1 km, **c** 4 km. In each frame, color-coded plots are given for all five values of the source half-width b. Symbols as in Figure 4

$$v_z(x, z; t) = -\frac{\zeta_0}{\pi} \int_0^\infty \frac{\cos kx \sin kb}{k \cosh kh} \cdot \frac{\sinh k(h+z)}{\sinh kh} \cdot$$

$$\frac{\kappa^2}{\kappa^2 - \omega^2} \cdot$$

$$\cdot \, [\omega \sin \omega t - \kappa \sin \kappa t$$
$$+ H(t - T)(\omega \sin \omega (t - T) + \kappa \sin \kappa t)] \cdot dk$$

$$(23)$$

(note that the conservation of mass is easily verified since $\partial v_x/\partial x + \partial v_z/\partial z = 0$, and similarly, $\partial v_x/\partial z = \partial v_z/\partial x$ expresses that the flow is irrotational). The local density (per unit length along x and y) of kinetic energy along the wavefront is then obtained as

$$e^{Kin} = \frac{\rho}{2} \int_{-h}^0 (v_x^2 + v_z^2) \cdot dz \qquad (24)$$

Similarly, the local density of potential energy is

$$e^{Pot} = \frac{\rho g}{2} \eta^2 (x_{Far}; t) \qquad (25)$$

The total energy of the tsunami, E^{Total} (per unit length along the y direction) is simply the integral over time of the total flux of kinetic and potential energy through the wavefront at x_{Far}:

$$E^{Total} = 2 \int_0^\infty (e^{Kin} + e^{Pot}) \cdot U \cdot dt \qquad (26)$$

where U is the group velocity of the wave. The factor 2 in (26) accounts for the contribution of the wave

propagating towards negative x. Note that since the wave is dispersed outside the SWA, different components of the integrand in (18) will travel with different group velocities:

$$U(k) = \frac{d\omega}{dk} = \frac{g}{2\omega} \left[\tanh kh + kh (1 - \tanh^2 kh) \right] \tag{27}$$

Assuming that no energy is exchanged across wavenumbers k, it is possible to circumvent this difficulty by directly multiplying the integrands in (18), (22) and (23) by $(U^{1/2})$. In all cases, we choose x_{Far} large enough that the wave has not yet reached it when the deformation at the source is complete $(t = T)$; in practice x_{Far} is at least 20 km, but can be as large as 90 km for the longest rise times and deepest oceans. Finally, we have verified numerically that the contributions of (24) and (25) are equal (generally to within 1%), as expected since at any given point, the energy of the tsunami oscillates between its kinetic and potential forms.

The values of E^{Total} are plotted as the solid triangles on Figs. 4 and 5, color-coded with the same conventions as E^{TSU} and E^{SWA}.

3.2. The Cylindrical Case

Another class of models investigated by Hammack (1972) is set in three-dimensional space with cylindrical symmetry, and considers a circular plug of radius r_0 on the ocean floor (green labels on Fig. 2). The equations of hydrodynamics are solved in a system of cylindrical polars, with the spatial Fourier transform replaced by a Hankel transform of order 0 $(r \to k)$:

$$\hat{\zeta}(k; t) = \int_0^\infty J_0(kr)\, \zeta(x; t) \cdot r\, dr \tag{28}$$

followed by the same temporal Laplace transform, eventually leading to (Hammack 1972; Eq. (3.102)):

$$\eta(r; t) = \int_0^\infty \frac{k\, J_0(kr)}{\cosh kh}$$
$$\left[\frac{1}{2i\pi} \int_{Br.} e^{st} \cdot \frac{s^2}{s^2 + \omega^2}\, \widetilde{\widehat{\zeta}}(k; s) \cdot ds \right] \cdot dk \tag{29}$$

replacing Equation (14), and in which $\widetilde{\widehat{\zeta}}$ is the double Hankel-Laplace transform of ζ. In these equations, J_v is the standard Bessel function of order v. Assuming the same rise time function for the plug, the deformation of the floor is now given by

$$\zeta(r; t) = \zeta_0 H(r_0 - r) \cdot \left[\frac{1}{2}(1 - \cos \kappa t) \right.$$
$$\left. H[t(T - t)] + H(t - T) \right] \tag{30}$$

and our computations are simply adapted to the new cylindrical symmetry, following Hammack (1972). Equations (18) and (19) are replaced by

$$\eta(r; t) = \frac{\zeta_0 r_0}{2} \int_0^\infty \frac{J_0(kr)\, J_1(kr_0)}{\cosh kh} \cdot \frac{\kappa^2}{\kappa^2 - \omega^2} \cdot$$
$$\cdot \left[\cos \omega t - \cos \kappa t + H(t - T)(\cos \omega(t - T) \right.$$
$$\left. + \cos \kappa t) \right] \cdot dk \tag{31}$$

and

$$p(r; t) = \frac{\rho g \zeta_0 r_0}{2} \int_0^\infty$$
$$\frac{J_0(kr)\, J_1(kr_0)}{\cosh^2 kh} \cdot \frac{\kappa^2}{\kappa^2 - \omega^2} \cdot$$
$$\cdot \left[\cos \omega t - \cos \kappa t + H(t - T) \right.$$
$$\left. (\cos \omega(t - T) + \cos \kappa t) \right] \cdot dk \tag{32}$$

while the energy of the tsunami (this time in actual units of energy) now takes the form

$$E^{TSU} = \pi \zeta_0 \kappa \int_0^{r_0} r\, dr \int_0^T p(r; t) \cdot \sin \kappa t \cdot dt \tag{33}$$

We compare it to E^{Static} and E^{SWA} now given by

$$E^{Static} = \frac{\rho g}{2} \int_0^{r_0} 2\pi r\, dr \left[\zeta(r; T) \right]^2 dt$$
$$= \frac{1}{2} \rho g \pi r_0^2 \zeta_0^2 \tag{34}$$

and

$$E^{SWA} = \pi \rho g \zeta_0 \kappa \int_0^{r_0} r\, dr \int_0^T \eta(r; t)\, \sin \kappa t \cdot dt \tag{35}$$

Similarly, in the far field, at distance r_{Far}, Eqs. (22) and (23) are replaced by

$$
\begin{aligned}
v_r(r, z; t) = & \; \frac{\zeta_0 r_0}{2} \int_0^\infty \\
& \frac{J_1(kr) J_1(kr_0)}{\cosh kh} \cdot \\
& \frac{\cosh k(h+z)}{\sinh kh} \cdot \frac{\kappa^2}{\kappa^2 - \omega^2} \cdot \\
& \cdot [\omega \sin \omega t - \kappa \sin \kappa t \\
& + H(t-T)(\omega \sin \omega(t-T) + \kappa \sin \kappa t] \cdot dk
\end{aligned}
\tag{36}
$$

$$
\begin{aligned}
v_z(r, z; t) = & -\frac{\zeta_0 r_0}{2} \int_0^\infty \frac{J_0(kr) J_1(kr_0)}{\cosh kh} \cdot \\
& \frac{\sinh k(h+z)}{\sinh kh} \cdot \frac{\kappa^2}{\kappa^2 - \omega^2} \cdot \\
& \cdot [\omega \sin \omega t - \kappa \sin \kappa t \\
& + H(t-T)(\omega \sin \omega(t-T) + \kappa \sin \kappa t] \cdot dk
\end{aligned}
\tag{37}
$$

which again satisfy $\mathrm{div}\,\mathbf{v} = 0$ and $\mathbf{curl}\,\mathbf{v} = \mathbf{0}$. The total tsunami energy (in units of energy) is the integral over time t of the energy flux through the circular wavefront at radius r_{Far}

$$
\begin{aligned}
E^{Total} = & \; 2\pi r_{Far} \rho \cdot \int_0^\infty U \\
& \cdot \left[\frac{1}{2}(v_r^2 + v_z^2) + \frac{1}{2} g \eta^2(r_{Far}; t) \right] \cdot dt
\end{aligned}
\tag{38}
$$

the dispersion of U with k being similarly taken into account by multiplying the integrands in (31), (36) and (37) by the square root of U, given by (27)

Figures 6 and 7 are exact counterparts to Figs. 4 and 5 in the new case of cylindrical symmetry.

4. Discussion

Figures 4 5 6 and 7 plot the ratio of the tsunami energy E^{TSU} scaled to its classic value E^{Static} computed under the assumption $\eta = \zeta$, as a function of the rise time of the source, each of them for 60

different scenarios, with additional cases computed at intermediate half-widths b (or radii r_0) and depths h. The value of the ratio E^{TSU}/E^{Static} expresses the energetic efficiency as a tsunami source of the particular model considered.

Our first result is the excellent agreement between the energy E^{TSU} estimated from Eq. (9) and its value computed by integrating its flux in the far field.

As expected, the tsunami efficiency is found to decrease with increasing rise time in all scenarios, which is in line with results obtained through numerical simulations for the surface amplitudes η (e.g., Derakhti et al. 2019). This simply expresses that for long rise times, the initial deformation cannot be fully grown at the surface, since the tsunami has the time to evacuate substantial amounts of displaced water outside the source area before the floor can reach its full deformation.

4.1. Applicability of the Shallow Water Approximation

We first discuss the effect of dispersion on the tsunami efficiency by further scaling E^{TSU} to its value obtained under the Shallow-Water Approximation, E^{SWA} given by (12). The ratio E^{SWA}/E^{TSU}, which is always larger than 1, can be used to quantify this effect through the dimensionless variable

$$\Omega = \cosh^{-1}\left(E^{SWA}/E^{TSU} \right) \tag{39}$$

that constitutes an inverse measure of the quality of the SWA, which will be valid for $\Omega \to 0$ but deteriorate with growing Ω. For any given ocean depth h, Ω can be interpreted through an equivalent, or dominant, wavenumber $K = \Omega/h$. The latter will of course be a complex combination of the source size (b or r_0), the depth h of the ocean, and the rise time T of the source. The parameter Ω is also a measure of the separation between the solid curves (E^{TSU}) and the open squares (E^{SWA}) on Figs. 4, 5, 6 and 7.

We plot on Fig. 8 the parameter Ω as a function of the square root of the ratio of ocean depth to source size (h/b in translational symmetry, or h/r_0 in cylindrical symmetry). We find that Ω follows a two-stage behavior: for large κ (short rise times T), it grows linearly, which means that the dominant wavenumber K is inversely proportional to the
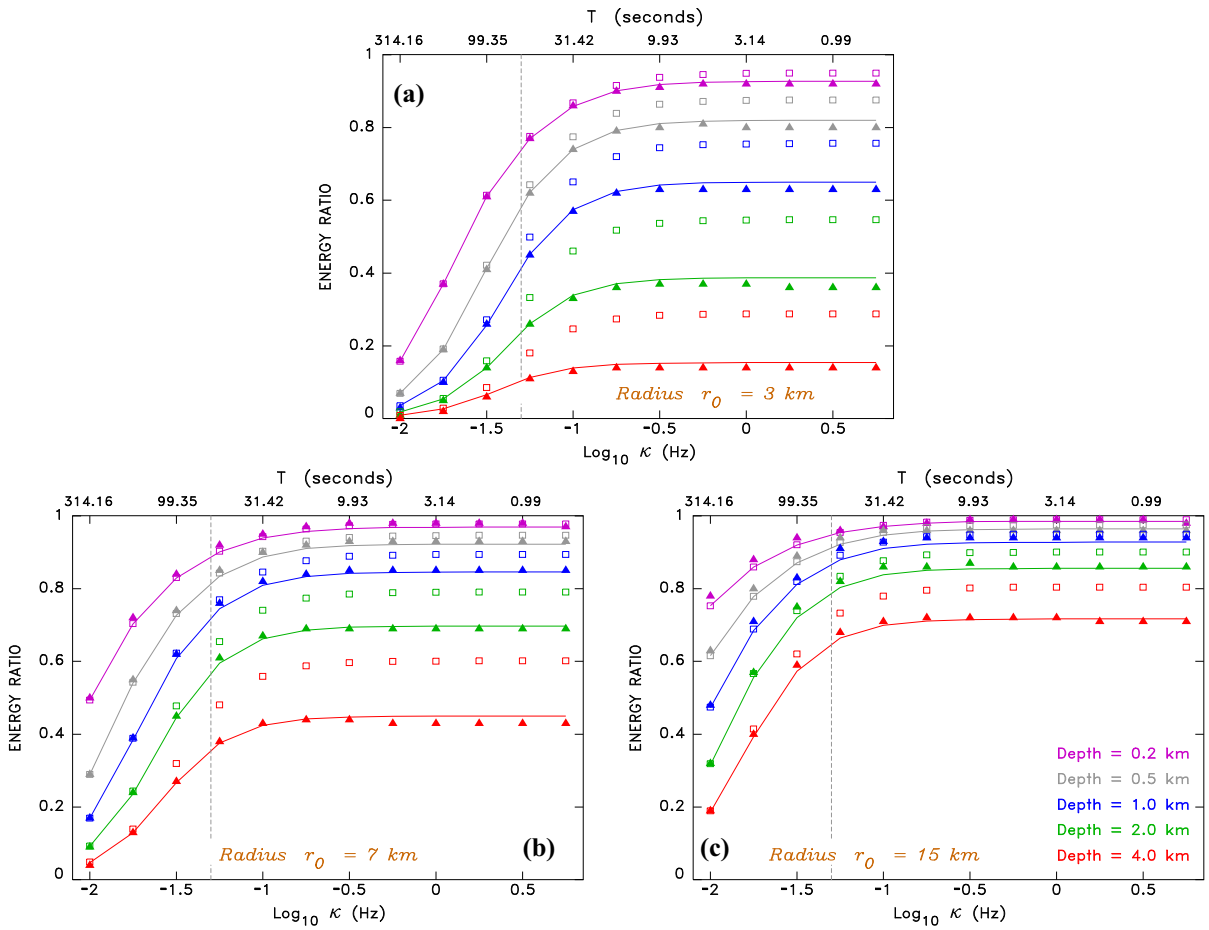
Figure 6
Same as Figure 4 for radial symmetry for source radii $r_0 = 3$ km (**a**), 7 km (**b**), and 15 km (**c**)

geometrical mean of source size and water depth. As κ decreases (and T increases), the duration of the source plays a growing role in controlling the dominant wavenumber and the parameter Ω, whose values are reduced (especially in the 2–D case); the SWA is then better verified. We find empirically that the change in behavior occurs in our geometries for the three largest values of T. That threshold, $T_t \approx 60$ s, shown as a grey vertical dashed line on Figs. 4, 5, 6 and 7, corresponds grossly to the elbows ending the flat regime of constant ratios E^{TSU} / E^{Static} for the various curves on those figures. Data points beyond T_t are shown as light grey symbols on Fig. 8.

We then regress the datasets for the 9 largest values of κ and obtain

$$\begin{aligned} \Omega &= 0.643 \sqrt{h/b} \quad (2\text{--D}) \quad \text{or} \quad \Omega \\ &= 0.981 \sqrt{h/r_0} \quad (3\text{--D}) \end{aligned} \tag{40}$$

which suggests the extremely simple result that, for this range of solutions, the dominant wave number K is given approximately by the inverse of the geometrical mean of source radius and depth, $\sqrt{r_0 h}$ (3–D) or of total source width and depth, $\sqrt{2b h}$ (2–D). However, as the ratio h/b is increased, Ω features a faster growth, resulting in a curvature of the distribution, particularly in the case of the 3–D circular source. We have verified that this curvature, which can be modeled with the parabolic functions
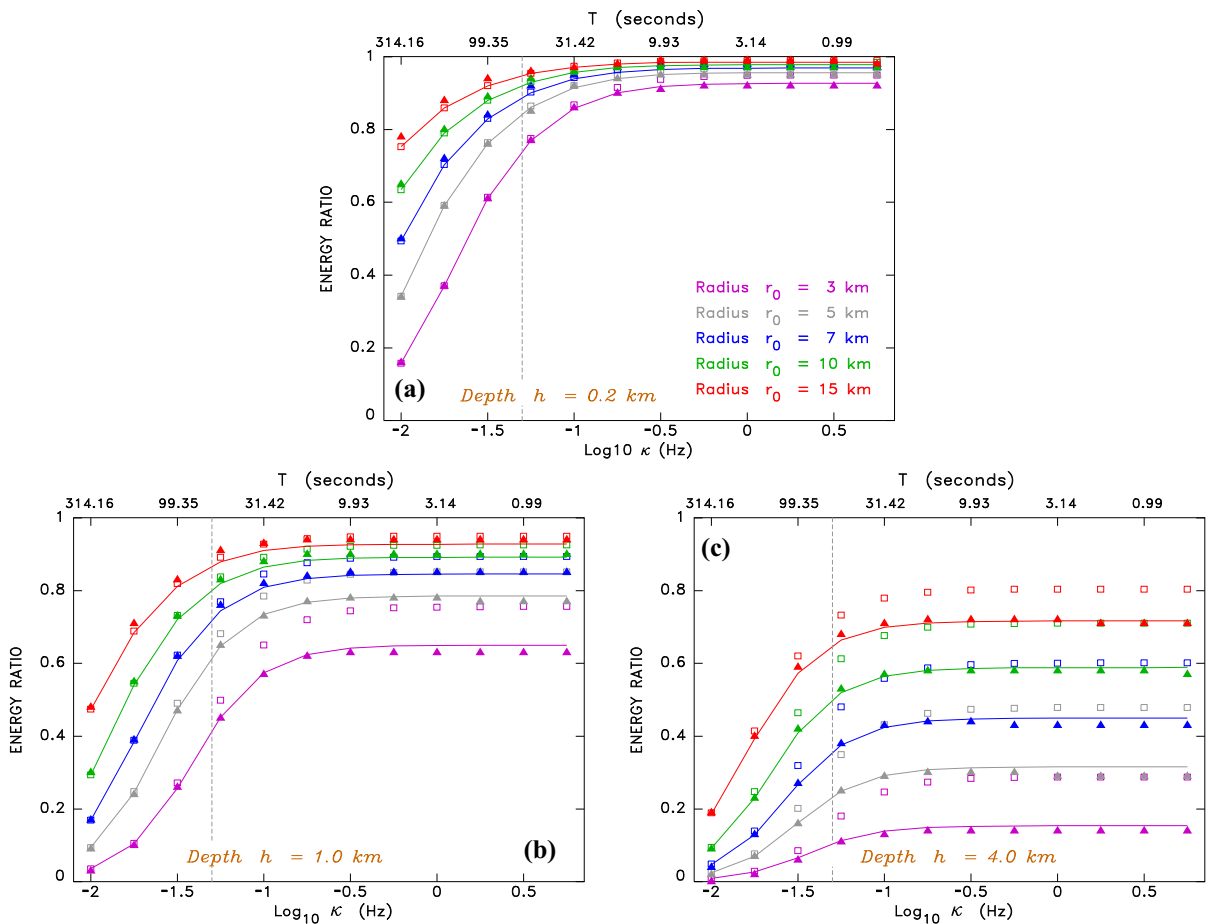
Figure 7
Same as Fig. 5 for radial symmetry and all five source radii

$$\Omega = 0.551 \sqrt{h/b} + 0.126 (h/b) \quad (2\text{--}D)$$
(41a)

or

$$\Omega = 0.781 \sqrt{h/r_0} + 0.275 (h/r_0) \quad (3\text{--}D)$$
(41b)

is statistically significant since in both cases, it passes an F–test (Dixon and Massey 1969) at the 99% level ($F = 147$ (2–D) and 284 (3–D) $vs.$ $F_{99} = 6.72$ for 225 points regressed with 2 $vs.$ 1 degrees of freedom). Finally, we note that in all cases, the parameter Ω is larger, and hence the SWA poorer, for the radial symmetry than for the translational one.

In summary, the domain of applicability of the SWA for the computation of tsunami energy is controlled by two independent factors: for fast rise times $T < T_t$, the equivalent wavenumber K is governed by the combination of h and the size of the source (b or r_0); while for slow rise times $T > T_t$, their influence becomes predominant in controlling K and Ω.

4.2. The limiting case of the instantaneous source ($\kappa \to \infty$ or $T \to 0$)

We now explore in detail the behavior of the efficiency ratio E^{TSU} / E^{Static} for large κ (fast sources with short rise times): it goes asymptotically to a
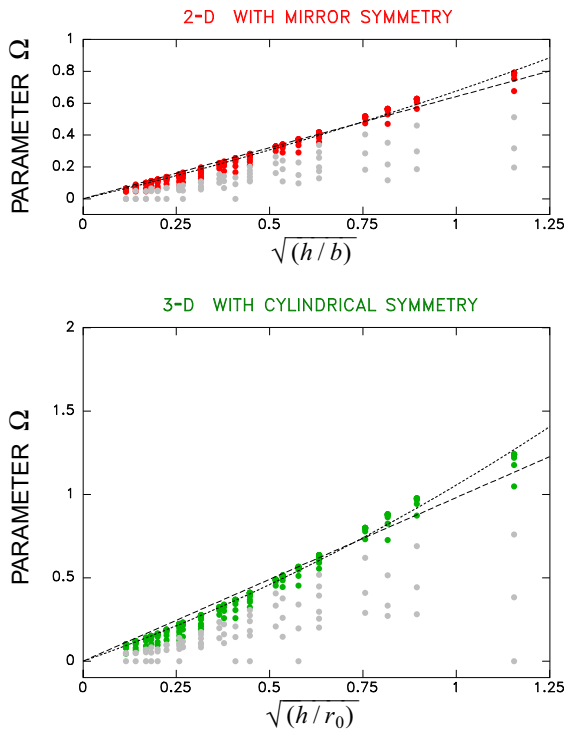
Figure 8
Dispersion parameter Ω, defined in (39) as a function of the square root of the ratio of water depth to source size, in the two-dimensional *(Top)* and three-dimensional *(Bottom)* geometries. The light grey points correspond to small values of κ (rise times $T > 60$ s). With these points excluded, the dashed lines are linear regressions of the datasets, and the dotted lines quadratic ones. See text for details

constant value R_{lim}, which is contoured on Fig. 9 as a function of ocean depth h and source size (b or r_0).

The most important result of our study is that R_{lim} can be significantly less than 1, for large values of h and/or small values of b (or r_0). Under such conditions, it is in simple terms impossible to reach full efficiency (*i.e.,* to pump into the tsunami the full energy predicted by the simple formula (10)), even for sources with instantaneous rise times. These results generalize to the concept of tsunami energy the so-called "Kajiura effect" (Kajiura 1963) expressing the influence of the ratio of source size to water depth on the amplitude of a tsunami wave over a point source.

We further examine quantitatively the issue on Fig. 10 by plotting R_{lim} as a function of the ratio (h/b) for the 2–D models, or (h/r_0) in the cylindrical ones.

In the first case (plotted in red), we find a remarkably linear dependence, regressing as

$$R_{lim} = 1 - 0.507\,(h\,/\,b) \qquad (42)$$

shown as the red long-dashed line on Fig. 10. An improved estimate is obtained, especially for large h/b, with the quadratic expression

$$R_{lim} = 1 - 0.645\,(h\,/\,b) + 0.151\,(h\,/\,b)^2 \quad (43)$$

(red dotted line), which provides a statistically better fit ($F = 383$ *vs.* $F_{99} = 7.74$ (Dixon and Massey 1969)).

In the case of the 3-dimensional cylindrical source, our results (in green on Fig. 10) indicate a stronger decay of R_{lim} with ($h\,/\,r_0$), regressed linearly as

$$R_{lim} = 1 - 0.810\,(h\,/\,r_0) \qquad (44)$$

(green long-dashed line on Fig. 10), and quadratically as

$$R_{lim} = 1 - 1.182\,(h\,/\,r_0) + 0.409\,(h\,/\,r_0)^2$$
$$(45)$$

(green dotted line), indicating a faster decay of R_{lim}, but also with more curvature ($F = 5123$).

Such variations of R_{lim} with the various geometrical scales of the problem can be understood at least qualitatively as follows. Values of R_{lim} less than 1 express the fact that, even for an instantaneous deformation of the ocean floor, the displaced water fails to reach the surface in the form of an equivalent hump. In a liquid taken as incompressible, that water flows laterally out of the source area. A dimensional argument suggests that, in the 2-dimensional model and again, per unit length in the direction y, the volume of water in question is proportional to b. It leaks laterally out of the source area through its edge whose surface is proportional to h, suggesting that the fraction of water not contributing to the tsunami energy, $(1 - E^{TSU}\,/\,E^{Static})$, will be indeed controlled by the ratio ($h\,/\,b$). In the cylindrical model, the volume of displaced water is proportional to $\pi\,r_0^2$ and the lateral surface is $2\pi\,r_0\,h$, leading again to R_{lim} controlled by ($h\,/\,r_0$). However, that dependence is slower than linear, as clearly verified in both cases using the F–tests. Finally, for any given ratio h/b or
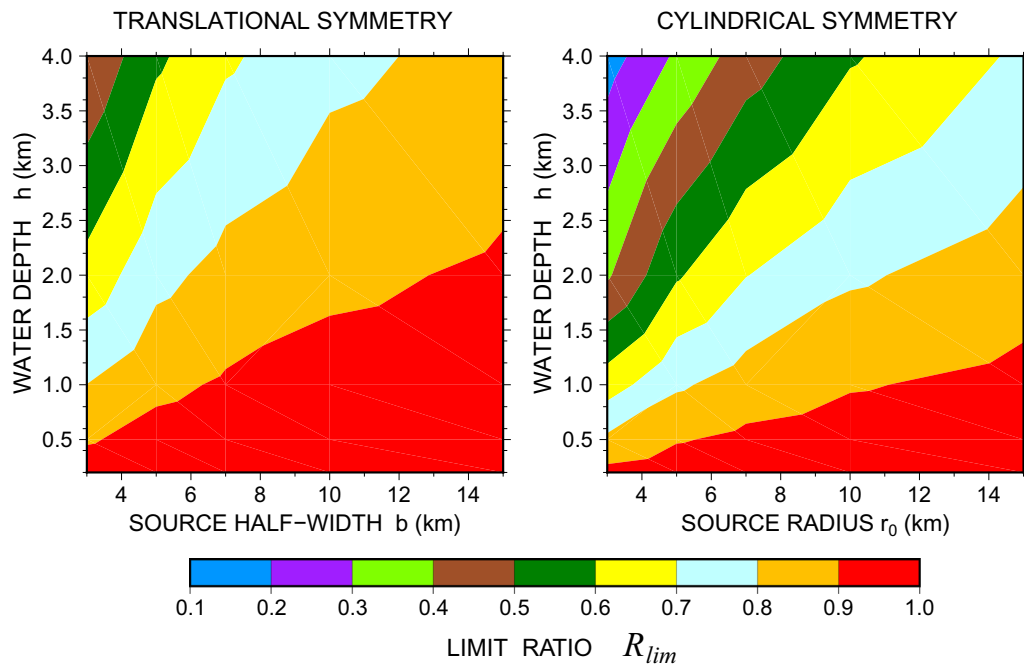
Figure 9
Contour plots of the function $R_{lim} = \lim\limits_{\kappa \to \infty} (E^{TSU} / E^{Static})$ as a function of depth h and half-width b (or radius r_0) of the source (both in logarithmic coordinates). Note that R_{lim} grows with b (or r_0) and $1/h$, and is always larger for the 2-dimensional geometry

h/r_0, the cylindrical model is less efficient at generating a tsunami, which simply expresses that the water can escape laterally in all azimuths (*i.e.,* in two dimensions), whereas in the 2-dimensional model, with its tacit translational symmetry along *y*, it can leak only in the *x* direction.

4.3. *Application to Realistic Earthquake Sources*

While our new results are interesting from a theoretical standpoint, they may bear only little direct application to the case of realistic tsunamigenic earthquakes, especially great ones. Because earthquake sources generally feature rise times much shorter than the periods of the tsunamis they generate, one generally considers as appropriate the "static" assumption of a direct transfer of the full displacement $\zeta(T)$ to the surface as a field of initial conditions $\eta(t = 0_+)$ for numerical simulations. However, we have seen above that the high-frequency limit of the tsunami efficiency E^{TSU} / E^{Static} is

controlled not only by rise time ($T = \pi/\kappa$), but also by the geometrical parameters of the models.

For a large seismic source, the situation is made complex by the heterogeneity of the bottom displacement field, ζ, on account both of the double-couple nature of the source which leads to a complex distribution of uplift and subsidence (Mansinha and Smylie [1971]; Okada [1985]), and of the occasionally strong heterogeneity of the slip Δu on the fault plane, as exemplified during the 2011 Tohoku mega-thrust event (Lay et al. [2011]). Nevertheless, the models studied above provide a framework for discussion. In general, the fault length L is much larger than its width W, and thus the 2-dimensional model may be more directly applicable than its cylindrical counterpart. For large earthquakes, $W = 2b$ is at least several tens of km (and up to 200 km for truly gigantic sources), and thus the ratio h/b remains small, on the order of at most 1/3 and usually much less, for a 5–km deep ocean. Figure [10] then suggests that the energy efficiency of the source would be at
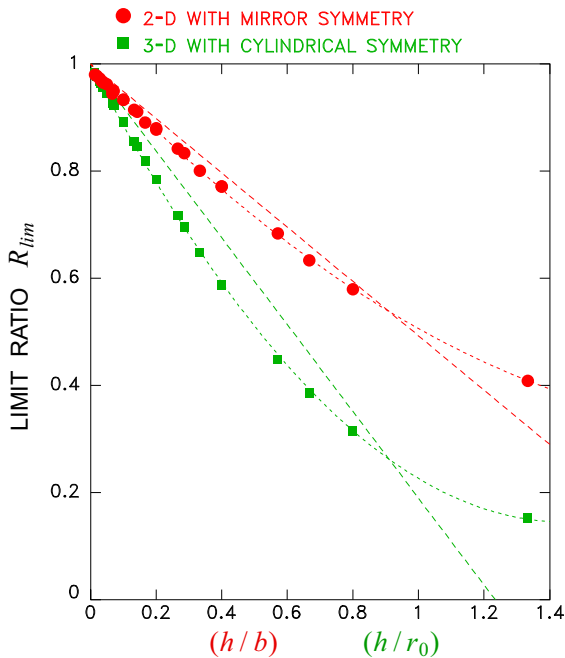
Figure 10

Dependence of R_{lim} on the depth-to-size ratios (h/b) (2-dimensional case; red) or (h/r_0) (cylindrical case; green). Dashed lines are linear regressions, and dotted lines quadratic ones; see text for details

least 85 to 90% (amounting to at least 92% in amplitude) with respect to the widely used "static" assumption.

At the lower end of the spectrum of seismic sources, strongly deficient tsunami efficiency (on the order of 50% or less) would require ratios $h/b > 1$, or $h/r_0 > 0.5$ in the cylindrical geometry which may be more applicable to smaller seismic sources; this would translate into seismic widths on the order of $W \leq 20$ km in very deep waters ($h = 5$ km), and even less (8 km) in shallower ones ($h = 2$ km). In turn, under global scaling laws (Geller 1976), this would correspond to seismic moments $M_0 \leq 5 \times 10^{26}$ dyn*cm in deep water, and $M_0 \leq 3 \times 10^{25}$ dyn*cm in shallow ones ($M_w \leq 7.0$ and 6.3, respectively). While the former could generate observable tsunamis, their effects would be constrained to the near field where wave amplitudes are directly related to local slip on the fault, and the concept of tsunami energy, integrated over the source area, loses its

interest. We conclude that under most operational conditions, large earthquake tsunamis with destructive effects in the far field will not be affected by the limit to tsunami efficiency outlined in this study.

The application of this approach to the more complex case of an underwater landslide will be the subject of a separate study.

Acknowledgements

References

Ben-Menahem, A., & Singh, S. J. (1981). *Seismic waves and sources*. New York: Springer.

Boas, M. (1983) *Mathematical methods in the physical sciences,* 820 pp., J. Wiley & Sons, New York.

Boatwright, J., & Choy, G. L. (1986). Teleseismic estimates of the energy radiated by shallow earthquakes. *Journal of Geophysical Research*, *91*, 2095–2112.

Dean, R.G., & Dalrymple, R.A. (2000). *Water wave mechanics for engineers and scientists,* 353 pp., World Scientific, Singapore.

Derakhti, M., Dalrymple, R. A., Okal, E. A., & Synolakis, C. E. (2019). Temporal and topographic source effects in tsunami generation. *Journal of Geophysical Research Oceans*, *124*, 5270–5288.

Dixon, W. J., & Massey, F. J, Jr. (1969). *Introduction to statistical analysis* (3rd ed.). New York: McGraw-Hill.

Dutykh, D., & Dias, F. (2009). Energy of tsunami waves generated by bottom motion. *Proceedings of the Royal Society of London, Series A*, *465*, 725–744.

Geller, R. J. (1976). Scaling relations for earthquake source parameters and magnitudes. *Bulletin of the Seismological Society of America*, *66*, 1501–1523.

Gill, A.E. (1982) *Atmosphere-ocean dynamics,* 662 pp., Academic Press, New York.

Hammack, J.L. Jr. (1972). Tsunamis – A model of their generation and propagation, *Ph.D. Dissertation,* 261 pp., California Institute of Technology, Pasadena.

Iida, K. (1963). A relation of earthquake energy to tsunami energy and the estimation of the vertical displacement in a tsunami source. *Journal of Earth Sciences of Nagoya University*, *11*, 49–67.

Kajiura, K. (1963). The leading wave of a tsunami. *Bulletin of the Earthquake Research Institute of Tokyo University*, *41*, 535–571.

Kajiura, K. (1981). Tsunami energy in relation to parameters of the earthquake fault model. *Bulletin of the Earthquake Research Institute of Tokyo University*, *56*, 415–440.

King, G. C. P. (1978). Geological faults, fractures, creep and strain. *Philosophical Transactions of the Royal Society of London*, *288*, 197–212.

Lay, T., Ammon, C. J., Kanamori, H., Xue, L., & Kim, L. J. (2011). Possible large near-trench slip during the 2011 $M_w = 9.0$ off the Pacific coast of Tohoku earthquake. *Earth, Planets and Space*, *63*, 687–692.

Mansinha, L., & Smylie, D. E. (1971). The displacement fields of inclined faults. *Bulletin of the Seismological Society of America*, *61*, 1433–1440.

Munk, W. H. (1963). Some comments regarding diffusion and absorption of tsunamis. *Proceedings of the Tenth Pacific Science Congress, IUGG Monograph*, *24*, 53–72.

Okada, Y. (1985). Surface deformation due to shear and tensile faults in a half-space. *Bulletin of the Seismological Society of America*, *75*, 1135–1154.

Okal, E. A. (2003). Normal modes energetics for far-field tsunamis generated by dislocations and landslides. *Pure and Applied Geophysics*, *160*, 2189–2221.

Okal, E. A., & Synolakis, C. E. (2003). A theoretical comparison of tsunamis from dislocations and landslides. *Pure and Applied Geophysics*, *160*, 2177–2188.

Rabinovich, A. B., Candella, R. N., & Thomson, R. E. (2013). The open ocean energy of three recent trans-Pacific tsunamis. *Geophysical Research Letters*, *40*, 3157–3162.

Saito, T. (2017). Tsunami generation: validity and limitations of conventional theories. *Geophysical Journal International*, *210*, 1888–1900.

Titov, V., Kânoğlu, U., & Synolakis, C. (2016). Development of MOST for real-time tsunami forecasting, *Journal of Waterway, Port, Coastal and Ocean Engineering, 142, (6),* 03116004, 16 pp.

Van Dorn, W. G. (1984). Some tsunami characteristics deducible from tide records. *Journal of Physical Oceanography*, *14*, 353–363.

Ward, S. N. (1980). Relation of tsunami generation and an earthquake source. *Journal of Physics of the Earth*, *28*, 441–474.